

A. Huber, K. McCormick, P. Andrew, P. Beaumont, S. Dalley, J. Fink,
J.C. Fuchs, K. Fullard, W. Fundamenski, L.C. Ingesson, F. Mast,
S. Jachmich, G.F. Matthews, Ph. Mertens, V. Philipps, R.A. Pitts,
S. Sanders, W. Zeidner and JET-EFDA contributors

Upgraded Bolometer System on JET for Improved Radiation Measurements

“This document is intended for publication in the open literature. It is made available on the understanding that it may not be further circulated and extracts or references may not be published prior to publication of the original when applicable, or without the consent of the Publications Officer, EFDA, Culham Science Centre, Abingdon, Oxon, OX14 3DB, UK.”

“Enquiries about Copyright and reproduction should be addressed to the Publications Officer, EFDA, Culham Science Centre, Abingdon, Oxon, OX14 3DB, UK.”

Upgraded Bolometer System on JET for Improved Radiation Measurements

A. Huber¹, K. McCormick², P. Andrew³, P. Beaumont³, S. Dalley³, J. Fink²,
J.C. Fuchs², K. Fullard³, W. Fundamenski³, L.C. Ingesson⁴, F. Mast²,
S. Jachmich¹, G.F. Matthews³, Ph. Mertens¹, V. Philipps¹, R. A. Pitts⁵,
S. Sanders³, W. Zeidner² and JET-EFDA contributors*


¹*Institut für Plasmaphysik, Forschungszentrum Jülich GmbH, EURATOM Association,
Trilateral Euregio Cluster, D-52425 Jülich, Germany*

²*Max-Planck-Institut für Plasmaphysik, EURATOM Association, 85748 Garching, Germany*

³*Euratom/UKAEA Fusion Association, Culham Science Centre, Abingdon, Oxon OX14 3DB, UK*

⁴*FOM-Instituut voor Plasmafysica, Nieuwegein, The Netherlands*

⁵*CRPP, Association EURATOM-Confederation Suisse, EPFL, Lausanne, Switzerland*

* See annex of J. Pamela et al, "Overview of JET Results",
(Proc.  IAEA Fusion Energy Conference, Vilamoura, Portugal (2004)).

Preprint of Paper to be submitted for publication in Proceedings of the
SOFT Conference,

(Warsaw, Poland 11th – 15th September 2006)

ABSTRACT.

Two new main-vessel bolometric cameras (KB5) with horizontal and vertical views of the plasma cross-section have been installed on JET, providing a substantial upgrade in capabilities: more viewing chords (24 chords for each camera), higher energy range (up to 8keV), higher sensitivity ($\sim 6.2\text{V/W}$), lower noise and therefore lower detectable signals ($\sim 2\mu\text{W/cm}^2$ at a bandwidth of 200Hz), higher temporal resolution ($\sim 2\text{ms}$). In addition, three new dedicated divertor bolometer cameras (KB3) with twelve lines-of-sight in total, optimised views and technical improvements have replaced the old ones. The combination of KB3 and KB5 systems provides measurements with significantly improved spatial resolution, allowing the divertor and main chamber radiation fractions to be clearly resolved. The sensitivity measured with an in-situ electrical method matches very well with that obtained using a light source calibration. The deviation between the two methods is less than 7% and is in the range of the measurement accuracy. The experimentally measured geometric functions closely match those computed using the design values of geometry. Tomographic reconstructions of high density divertor plasmas with ITER-like configuration are presented which clearly demonstrate the capability of the new diagnostic.

1. INTRODUCTION

Partially detached divertor operation is mandatory to reduce strike point power fluxes in long pulse, high power fusion devices. The understanding of this complex detached state is still incomplete and requires 2D simulations which themselves rely on high quality experimental data to be properly constrained. The radiation distribution is particularly important, but is often poorly resolved in space and magnitude in the divertor region where it is most required. To improve the quality of such measurements on JET, two new main-vessel bolometric cameras with horizontal (KB5H) and vertical (KB5V) views of the plasma cross-section have been installed, providing a substantial upgrade in capabilities: more viewing chords, higher energy range, higher sensitivity, lower noise and therefore lower detectable signals. Both cameras collect the radiation along 24 chords, 8 of which in each case cross the divertor region and the region adjacent to the divertor with 8 cm separation between the chord axes (see Fig.1). The other 16 channels of both cameras cover the entire plasma. The lines-of-sight for KB5V are determined by the individual bolometer apertures in connection with a collimator block. In the case of the horizontal camera (KB5H), a more simple pinhole structure is used to define the lines-of-sight.

In addition to the main chamber system, three new dedicated divertor bolometers (KB3) with twelve lines-of-sight in total, optimised views and technical improvements have replaced the old ones. The remaining 4 older divertor cameras have been repaired. The combination of the divertor systems with the KB5 overview cameras leads to a substantial improvement in radiation pattern reconstructions, particularly in the divertor region.

2. TECHNICAL DETAILS

2.1 MAIN VESSEL BOLOMETRY

The detectors are miniaturised metal foil detectors, of the same design as those used on Tore-Supra [1], RFX [2-3], JET [4] and ASDEX-Upgrade [5]: an 8 μm -thick gold-absorbing layer on a 20 μm -thick mica substrate and a gold meander on the rear side with a typical resistance of 1.2k Ω . The absorbed power onto the foil is monitored by its temperature change and the consequent increase in resistance of the gold meander. To compensate for both temperature drifts and electromagnetic disturbances, a second reference bolometer is employed which is optically shielded from the plasma. The two reference meanders and two measurement meanders are coupled in a Wheatstone bridge circuit such that the output voltage is proportional to any momentary temperature excursion of the measuring absorber. Four such units are combined to form a bolometer head (see Fig.2). They are produced by IPT [6]. The active area of the absorbed foil is 3.8 \times 1.3mm² with a 5mm spacing between detectors. A thin thermally conducting, 0.2 μm thick layer of gold gives the absorbing foil contact with the body of the bolometer head.

The bolometers with an 8 μm -thick gold-absorbing layer are sensitive in the spectral range from 0.1nm \rightarrow 480nm, corresponding to a photon energy of \sim 10keV \rightarrow 2.5eV. Fig.3 compiles the absorption and reflection coefficients for gold in the energy range from 0.1eV \rightarrow 1keV, showing (Fig.3a) that the absorber reflects 38% of incident power at 2.5eV, falling to 2% at 50eV. At the high energy end (Fig.3b), the absorption coefficient decreases beyond 10keV (5keV for the old JET bolometers equipped with a 4 μm -thick gold-absorbing layer), but at 8keV, \sim 98% of the incident power is still absorbed. The absorbed power is transmitted to the resistor meander through the mica foil whose thickness thus determines the thermal response time of the bolometer, $\tau_r = x^2 C \rho / \lambda = 1.86\text{ms}$, which is essentially the heat transfer time across the foil. Here x , C , ρ and λ are respectively the thickness (20 μm), specific heat capacity (0.837J/gK), density ($2.906 \times 10^{-3}\text{kg/m}^3$) and thermal conductivity (0.52W/mK) of mica foil.

A 40V_{pp} (peak-to-peak voltage), 50 kHz sinusoidal voltage is applied separately to each bridge of the bolometer and the electronics amplifies the output (up to a factor of 5000) with a maximum bandwidth of 2kHz. The signal is then processed in order to calculate the incident power ($P(t)$) on the bolometer according to the bolometer equation [3]:

$$P(t) = \frac{\tau_C}{S_{\text{bolo}}} \left(\frac{d\Delta U(t)}{dt} + \frac{\Delta U(t)}{\tau_C} \right)$$

where $\Delta U(t)$ is the output voltage, S_{bolo} [V/W] is the sensitivity and τ_C (s) is the cooling time constant of the foil. The quantities S_{bolo} and τ_C are determined by the calibration of the instrument. Use of synchronous demodulation techniques with a carrier frequency of 50kHz and an improved shielding concept of bolometer (including the head, cables and electronics) has permitted a dramatic decrease in the detection limit (signal-to-noise ratio $S/N=1$) to $\sim 2\mu\text{W/cm}^2$ at a bandwidth of $\Delta f=200\text{Hz}$

(versus $70\mu\text{W}/\text{cm}^2$ at $\Delta f=10\text{Hz}$ for the old bolometry system). All 48 bolometer signals are made available to the Real Time Control system [9] for feedback/control purposes, with a maximum sampling bandwidth of 5kHz.

Each bolometer head has undergone stringent and extensive tests [10]. A baking cycle at 160°C for 6 hours with monitoring of bolometer properties has first been performed. Calibration of the bolometer foils to determine τ_C and S_{bolo} has been performed at ambient temperature, 80°C and 160°C . In addition, the noise level for a 1kHz bandwidth and amplifier gain of 5000 has been measured. The peak-to-peak noise level is less than 20mV. Neither τ_C nor S_{bolo} exhibit a clear temperature dependence. The values averaged over all KB5 bolometers are: $\tau_C \sim 202 \pm 29\text{ms}$ in vacuum, $\sim 99 \pm 7\text{ms}$ in air, and $S_{\text{bolo}} \sim 3.6 \pm 0.2\text{V/W}$ in air and $\sim 6.2 \pm 1.0\text{V/W}$ in vacuum. The temperature coefficient of the meanders is $dR/dT(1/R) \sim 2.1 \cdot 10^{-3} / ^\circ\text{C}$, with $R \sim 1200\text{-}1400\text{ W/meander}$. These are typical values for mica-based bolometer foils with the characteristics specified above.

Since in the past some JET bolometers have experienced RF interference during Lower Hybrid heating (LH-heating), it was important to validate the shielding capability of the bolometer heads and grounding system foreseen for KB5. Tests of JET bolometer heads on Tore-Supra (similar LH-heating system as JET) under normal operating conditions at the $P_{\text{LH}} \sim 3\text{MW}$ level revealed no RF influence on the bolometer signals [11].

Since the cameras are mounted close to the plasma, within a vessel heated to 220°C during operation and up to 340°C during bakeout and since the bolometer head will not withstand temperatures exceeding 140°C (mostly due to formation of microcracks in the mica substrate), active cooling is necessary. At JET, the main-vessel bolometers are water cooled with water flow rate of 1l/min, with which the bolometer heads can be maintained at $30\text{-}35^\circ\text{C}$ for water at 20°C . As a backup, air cooling is foreseen. Pt100 resistors continuously monitor the bolometer head temperatures. More information on cooling tests and analysis of material stresses due to strong eddy currents in the case of plasma disruptions can be found in [10].

2.2 DIVERTOR BOLOMETRY

The divertor bolometers are equipped with the same type of bolometer heads (four channels per head) as the main-vessel bolometers. In contrast to the latter, the divertor detectors do not have an active cooling system and must be able to withstand the highest bakeout temperature of 340°C . Since shrinking of the gold meander foil occurs earlier for thinner foils, the resistance of non-cooled bolometers has been chosen between 300 and 400W. The high temperature mica version (up to 350°C versus 140°C for main bolometer system) of the same thickness of $20\mu\text{m}$ has been provided. The gold-absorbing layer has a thickness of 4nm yielding a detector sensitive up to a photon energy of 5keV. A 28Vpp sinusoidal voltage at 20kHz is applied separately to each bridge of the bolometer with electronics amplifying the output (up to a factor of 5000) with a maximum bandwidth of 2kHz. For the new KB3 bolometers, τ_C varies between 160 and 189ms in vacuum and between 77 and 95ms in air. The sensitivity varies in the range between $S_{\text{bolo}} = 2.8 \rightarrow 5.1\text{V/W}$ in vacuum,

and $2.0 \rightarrow 3.5 \text{ V/W}$ in air. The lower sensitivity of divertor cameras is compensated by larger étendues ($0.6\text{-}1.0 \times 10^{-8} \text{ sr m}^2$ versus $1\text{-}7 \times 10^{-8} \text{ sr m}^2$ for main chamber systems).

3. ABSOLUTE BOLOMETER CALIBRATION

The bolometers must be absolutely calibrated regularly in-situ using an electrical technique [12], which is a standard calibration procedure on many tokamaks. A square wave excitation current is applied to the bolometer bridge to transfer a known quantity of ohmic heating to the bolometer foil and the time evolution of the bolometer response is measured. This allows τ_C and S_{bolo} to be determined. In order to verify the electrical calibration, the bolometers were optically irradiated with an absolutely calibrated UV light source coupled with an interference filter at $\lambda=365\text{nm}$ (the absorption coefficient of gold at this wavelength is about 0.62, see Fig.3a). These measurements have been performed at two different distances between the light source and the detectors (first aperture of the detection system): 150mm and 500mm. Photogrammetry has been used to position the light source at a given distance on the viewing cone axis of any given bolometer with accuracy below 0.1mm. The results of these measurements for both main vessel cameras and for the new divertor cameras are summarised in Fig.4, where the sensitivities of the electrical calibration (filled squares) are compared with those obtained by optical irradiation (filled triangles). Clearly, both methods agree well, with deviations of less than 7%, within the measurement accuracy.

4. GEOMETRICAL PROPERTIES OF DETECTION SYSTEM

Due to the finite detector aperture sizes, the 3D geometrical properties of the detection systems must be accounted for when performing 2D tomography. The most convenient way to describe the geometrical properties of the detection system is with the use of a geometric function. The geometric function in this case describes the solid angle spanned by the entrance pupil of the detection system for each position in the reconstruction plane (i.e. the plane in which the local emissivity is to be reconstructed). Because the viewing geometry (positions and sizes of detectors and apertures) is known accurately, geometric functions in reconstruction space can be calculated. However, a quantity such as reflection on the wall of the aperture can only be correctly analysed by measurement. Both the collimator and pinhole are blackened internally with Aquadag (18% No. 5-1543-0-131-20 from Acheson Industries Ltd.) to reduce internal reflections. A direct measurement of the absorbed power is possible when a sufficiently powerful light source is available in the spectral region of interest. Such measurements have been performed using a 1kW Hg (Xe) Lamp. A small quantity of Xe maintains the light flux at a constant level over a long time. It also leads to a reduction in the arc size (1mm \times 3mm) allowing the high efficiency light coupling into optical fibres. The light is collected and imaged onto an optical fibre with 1mm core size and numerical aperture of about $\text{NA}=0.22$. The spatial resolution of these measurements is defined by the size of this fibre and was thus 1mm. The power density at the fibre output has been measured with an absolutely calibrated radiometer, demonstrating that the light source is nearly isotropic inside the light cone defined by the fibre NA.

This point source of light (optical fibre) has been located on the axis of each detector viewing cone and moved in the reconstruction plane in both poloidal and toroidal directions. Figure 5 presents a series of measurements of normalised geometrical function $h(\xi, \theta=0)/h(\xi=0, \theta=0)$ for channels crossing the divertor region and includes for comparison the calculated values using the design geometry. The values x and q describe the poloidal and toroidal angles at which the light source is observed at the entrance pupil of the detection system. The experimentally measured geometric function is well reproduced by the calculated values. Figure 5 also clearly demonstrates how the geometric function has been optimised so that adjacent channels nearly overlap at the half maximum. In some cases, the small pedestal seen at the edges of the geometric function is likely to be caused by reflections on the aperture walls. These reflections lead at most to an overestimation of about 2% of signal and can be neglected.

The light yield of the detection system is characterised by its étendue (units: sr m^2), also known as throughput. A high accuracy calculation of étendue for each detector has been made. Details of how this calculation of the detection-system property may be performed may be found in [13].

Étendue for the 16 channels of each KB5 camera covering the main plasma varies between 2×10^{-8} and $7 \times 10^{-8} \text{ sr m}^2$. The 8 channels of each camera which cross the divertor region with finer spatial resolution (8cm separation between the chord axes) have an étendue of about $1 \times 10^{-8} \text{ sr m}^2$. The new divertor bolometers have the étendues in the range $0.6\text{-}1.0 \times 10^{-8} \text{ sr m}^2$.

5. EXAMPLE RESULTS OF FIRST MEASUREMENTS WITH THE NEW SYSTEM

A new operational campaign at JET has recently begun, with first attempts at producing high triangularity $d=0.5$, ITER-like plasma configurations. These discharges are ultimately intended to investigate Type I ELMy-H-modes at high input power and plasma current. They are particularly interesting from the divertor physics point of view with regard to the rather short inner divertor leg and the consequent proximity of the X-point to the inner divertor target. They also constitute the first high performance plasmas in which the new bolometer systems have been used.

Figure 5 shows the reconstructed radiation in an inter-ELM period (averaged over 10ms) in two separate discharges with differing magnetic field configuration (varying X-point and target strike point locations). The discharges have $B_T = 2.7\text{T}$, $I_p = 2.5\text{MA}$, 14.5MW and 3.0MW of NBI and ICRH power respectively, $q_{95} = 3.3$, \bar{n}_e/n_{GW} . In the discharge with the shortest X-point to inner target distance (Fig.6a), the ELM frequency was $f_{ELM} \sim 7\text{Hz}$. In the second, with larger X-point to inner target distance $f_{ELM} \sim 35\text{Hz}$. The improved time resolution of the new bolometry system allows tomographic inversion of the radiation distribution in-between ELMs to be performed. When the X-point is close to the divertor tile the ELMs are compound (Type I ELM followed by high frequency small type III ELMs) and the majority of the radiation is located at the X-point and at the inner strike point, with significant radiation inside the Last Closed Flux Surface (LCFS) above the X-point. A significant quantity of radiation is also concentrated in the outer divertor Scrape-Off Layer (SOL). A poloidal array of fixed Langmuir Probes (LP) in the inner and outer divertor targets

is used to measure local saturation current, electron density and temperature, T_e . At the inner strike point $T_e \sim 43\text{eV}$ and the inner divertor is attached. Moving the X-point away from inner divertor strongly affects the ELM behaviour and the radiation distribution (Fig.6b). The ELM frequency increases and clean type I ELMs are observed. An increase of diamagnetic stored energy from 5.5MJ to 6.25MJ is also observed. The radiation is mostly located outside the LCFS in the inner SOL as well as in the private flux region. P_{rad} averaged over 10ms in the inter-ELM period is $P_{\text{rad}} = 7.75\text{MW}$ (43% of P_{heat}) and the wall load in the divertor due to this radiation is $\approx 0.3P_{\text{rad}}$. During the ELM, the radiation is mostly located in the inner divertor region (not shown in the figure). Although the time dependence of the radiation during an ELM cannot be resolved, the improved time resolution of the new system allows an estimate of the total radiated energy (DE_{rad}) during the ELM. Using an algorithm similar to that described in [14], $\Delta E^{\text{rad}} = 50\text{kJ}$, corresponding to 30% of ELM-energy losses ($\Delta W_{\text{dia}}^{\text{ELM}} \approx 150\text{kJ}$).

SUMMARY

To improve the quality of bolometric measurements on JET, two new main-vessel cameras (KB5) with horizontal and vertical views of the plasma cross-section have been installed, providing a substantial upgrade in capabilities: more viewing chords (24 chords for each camera), higher energy range (up to 8keV), higher sensitivity ($\sim 6.2\text{V/W}$), higher temporal resolution ($\sim 2\text{ms}$), lower noise and therefore lower detectable signals ($\sim 2\mu\text{W}/\text{cm}^2$ at a bandwidth of 200Hz). In addition, three new dedicated divertor bolometers (KB3) with twelve lines-of-sight in total, optimised views and technical improvements have replaced the old ones. The combination of the divertor bolometers with the KB5 main-vessel cameras provides measurements with significantly improved spatial resolution, allowing the divertor and main chamber radiation fractions to be clearly resolved. The sensitivity measured with an in-situ electrical method closely matches that obtained with a light source calibration. The deviation between the two methods is less than 7% and is in the range of the measurement accuracy. The finite detector aperture sizes mean that the 3D geometrical properties of the detection systems must be taken into account for the purposes of 2D tomography. The experimentally measured geometric functions are found to closely reproduce those calculated using geometric design values.

Lower Hybrid RF tests on Tore-Supra have shown that these bolometers remain undisturbed. The enormous improvement in temporal resolution will allow all 48 bolometer signals to be made available to the Real Time Control System.

Preliminary results obtained at the beginning of the most recent JET experimental campaigns have clearly demonstrated the enhanced capability of the new diagnostic which, in addition to superior quality of spatial reconstructions in the divertor region, now allows sufficient time resolution for radiation dynamics in between and during ELMs to be resolved.

REFERENCES

- [1]. K.F. Mast, J.C. Vallet et al., "A Low Noise Highly Integrated Bolometer Array for Absolute Measurement of VUV and Soft X Radiation", *Rev. Sci. Instrum.* **62** (1991) 744.
- [2]. K.F. Mast et al., "Fast Bolometric Diagnostic in the RFX Reversed Field Pinch Experiment", *Rev. Sci. Instrum.* **63** (1992) 4714.
- [3]. A. Murari, K.F. Mast et al., "Multichord Calibrated Bolometer Array for the RFX Experiment", *Rev Sci Instrum.* **66** (1995) 665.
- [4]. R. Reichle, et al., "Bolometer for ITER," in *Diagnostics for Experimental Thermonuclear Fusion Reactors*, Plenum Press, New York, 1996, pp. 559-570.
- [5]. J.C. Fuchs, K.F.Mast et al., "Radiation Distribution and Power Balance in the ASDEX Upgrade LYRA Divertor", *ECA Vol. 22C* (1998) 1510-1513.
- [6]. IPT-Albrecht GmbH, Ing.-Büro für Physikalische Technik, Emmendingen, Germany
- [7]. H. J. Hagemann, W. Gudat and C. Kunz, *Deutsches Elektronen-Synchrotron*, Report DESY SR-74/7 May 1974.
- [8]. L.R. Canfield, A. Hass and W. R. Hunter, "Colloquium on the Optics of Solid Thin Layers, Marseilles, September 1963", *J. de Physique* **25** (1964) 124.
- [9]. E. Joffrin, et al., "Integrated Scenario in JET Using Real Time Profile Control", *Plasma Phys. Control. Fusion* **45** No 12A (2003) A367-A383.
- [10]. K. McCormick, A. Huber, C. Ingesson et al., "New bolometry cameras for the JET Enhanced Performance Phase" *Fusion Engineering and Design* **74** (2005) 679.
- [11]. J.C. Vallet, private communication
- [12]. A. Murari, M. Cecconello, L. Marrelli, K. F. Mast "Absolute calibration and error analysis for thin gold metal foil bolometers" *Rev Sci Instrum*, **75** (2004) 2692.
- [13]. L.C. Ingesson, C.F. Maggi and R. Reichle, "Characterization of geometrical detectionsystem properties for two-dimensional tomography", *Rev. Sci. Instrum.* **71** (2000) 1370.
- [14]. J.C. Fuchs, T. Eich, A. Hermann et al., "Radiation distribution and energy balance during type-I ELMs in ASDEX Upgrade", *J. Nucl. Mater.* **337-339** (2005) 756.

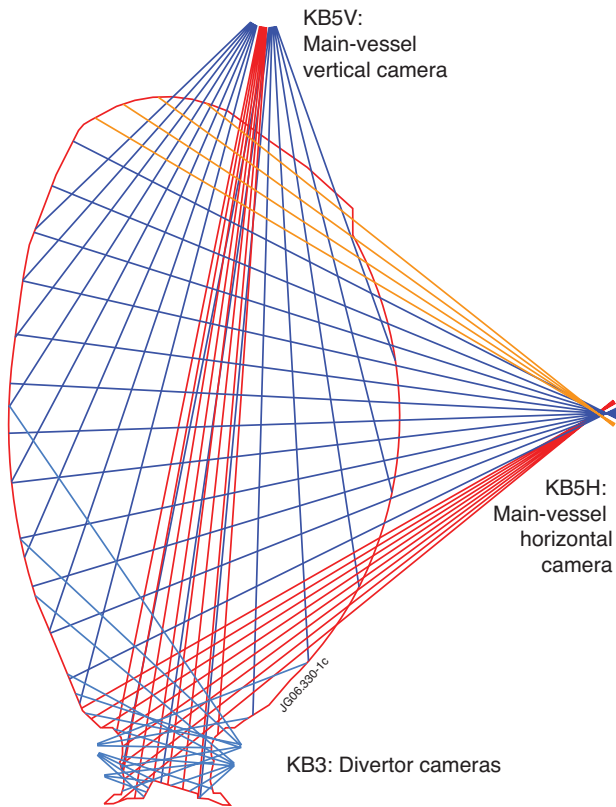


Figure 1: Lines-of-sight of the new bolometer system, including main chamber and divertor viewing systems.

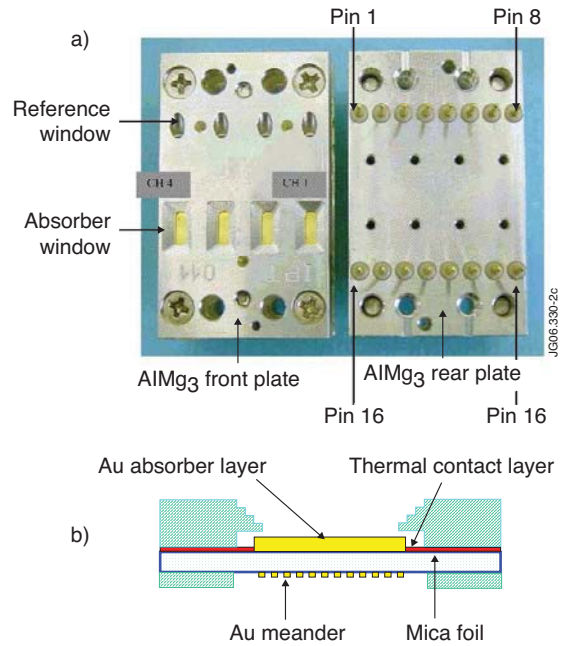


Figure 2: a) Four channel bolometer head b) schematic representation of the detector head crosssection.

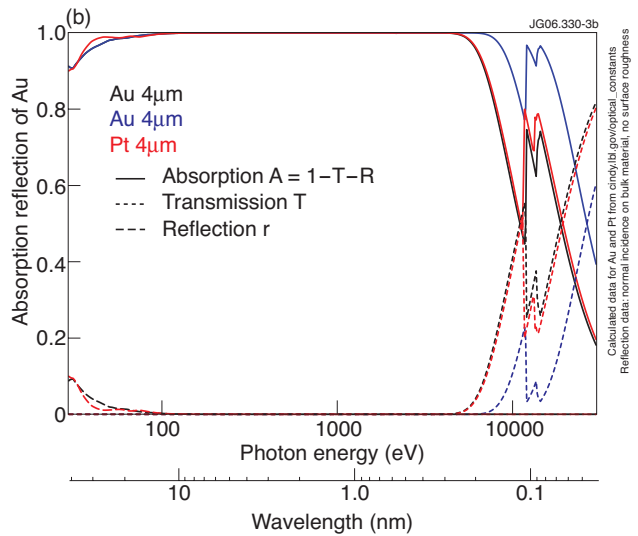
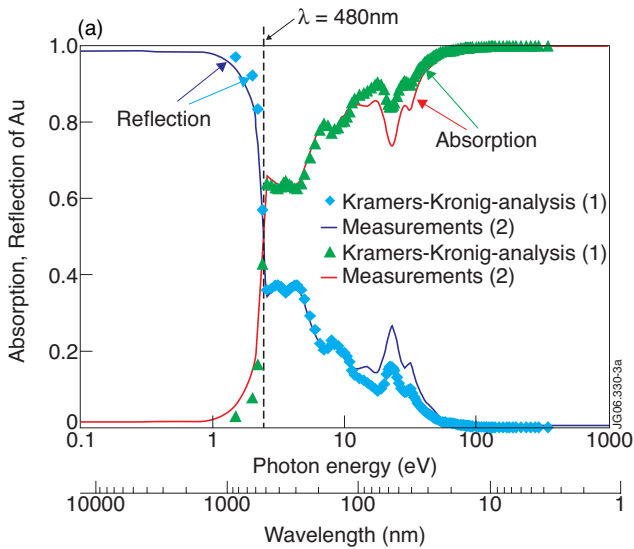


Figure 3: Absorption and reflection coefficients of gold in the energy range from 0.1eV to 10keV.

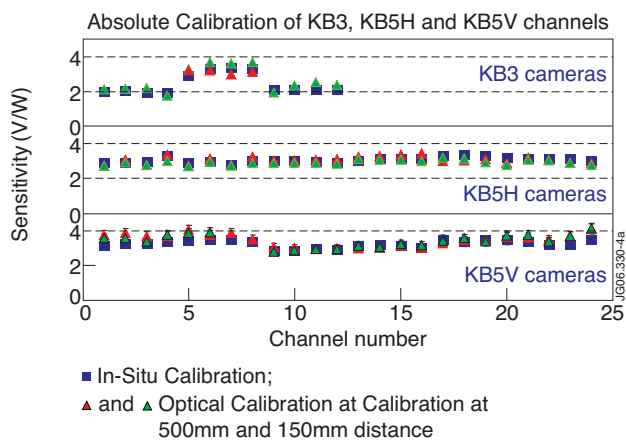


Figure 4: Detector sensitivities obtained from electrical calibration (filled squares) and optical irradiation (filled triangles).

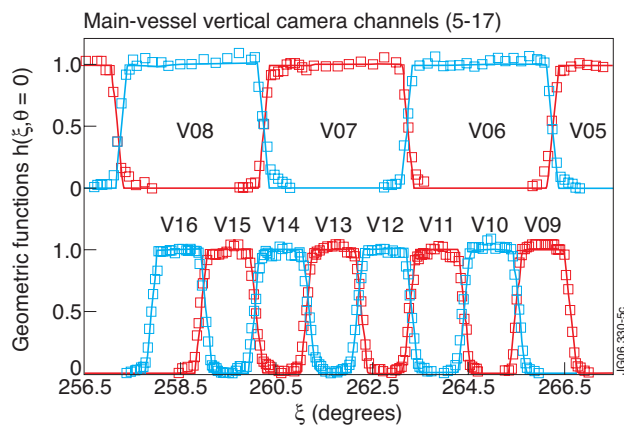


Figure 5: Normalised geometrical function $h(\xi, \theta = 0)/h(\xi = 0, \theta = 0)$ for KB5 channels crossing the divertor region in comparison with values calculated using the design values of geometry.

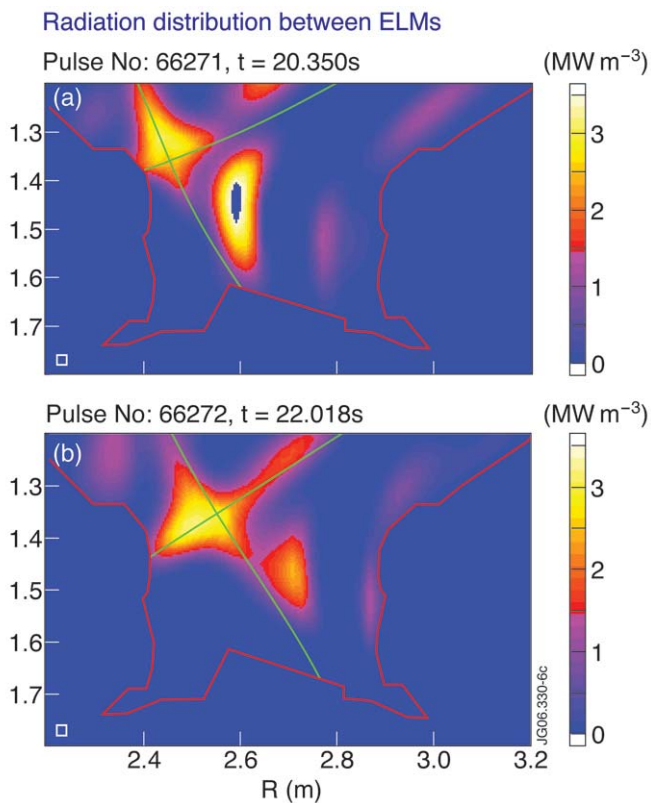


Figure 6: Total radiation distribution in between ELMS for two different magnetic field configurations.